Check for updates

The Journal of Engineering

*The 9th International Conference on Power Electronics, Machines and Drives (PEMD 2018)*

IET Journals
The Institution of Engineering and Technology

# Space modulation profile modelling for steer-by-wire SMPMSM

eISSN 2051-3305
Received on 26th June 2018
Accepted on 30th July 2018
E-First on 26th April 2019
doi: 10.1049/joe.2018.8248
www.ietdl.org

*Kris Scicluna*[1,2] ✉, *Cyril Spiteri Staines*[1], *Reiko Raute*[1]

[1]*Department of Industrial Electrical Power Conversion, University of Malta, Malta*
[2]*Institute of Engineering and Transport, Electrical and Electronics, Malta College for Arts, Science and Technology, Malta*
✉ *E-mail: Kris.Scicluna@mcast.edu.mt*

**Abstract:** This paper presents a sensorless estimation algorithm for steer-by-wire applications based on the injection of a high-frequency rotating voltage. Enhancement to the basic sensorless algorithm through SMP look-up tables is proposed. The improved observer was simulated in MATLAB for a 12 V RMS 400 W permanent magnet synchronous machine (PMSM).

## 1 Introduction

Steer-by-wire systems aim to minimise the number of mechanical linkages involved in steering, between the driver input (handwheel) and the vehicle output (wheels). The characteristics and safety requirements of steer-by-wire have been widely documented in literature [1–4]. The precision of sensor measurements in steer-by-wire has been identified as safety critical. Measurements include the electrical machines' currents, voltages, and rotor positions. The system currents/voltages are typically obtained from printed circuit board (PCB)-mounted transducers which have high accuracy and linearity throughout their operating range. The rotor position is obtained either through an optical or magnetic encoder. Optical encoders offer high resolution, however, tend to be prohibitive in terms of cost for automotive applications. Magnetic encoders have lower cost but are typically available up to 12-bit resolution. Both technologies have significant limitations when applied to steer-by-wire. Optical encoders tend to have reduced lifetime when subject to mechanical vibrations, which are commonly found in automotive applications. Magnetic encoders are non-contact and, therefore, are not worn out from mechanical rotation or vibrations. However, in this research, it was found that the linearity of commonly used low-cost magnetic encoders varies significantly with fractional millimetre variations in the air gap between the magnet mounted on the rotor shaft and the encoder sensing integrated circuit (IC).

Given the limitations of position sensors in practical steer-by-wire applications, it is required to include a backup measurement system to obtain the necessary automotive safety integrity level (ASIL) required by the automotive industry. Researchers typically introduce redundant encoders for backup in case of failure of the primary sensor. The drawback of this approach is that it increases both system cost and mechanical complexity of the steer-by-wire system. To date, the most advanced implementation of steer-by-wire in a production vehicle was in the infinity Q50, which included a redundant mechanical backup system due to safety concerns. Such a system relinquishes two main advantages of the steer-by-wire system: simplified mechanical design and unconstrained handwheel placement.

The research presented here proposes the use of sensorless estimation and control algorithms for encoder validation and backup. These algorithms estimate the rotor position from current and voltage measurements, which are integrated in standard position/current-controlled electrical drives. The electrical machines used in steer-by-wire are typically three-phase permanent magnet (PM) machines due to the high power density and low maintenance of these machines [5, 6]. While high-speed sensorless control of PM machines can be easily carried out with model-based observers operating on the back-emf of the machine [7], these are not applicable for steer-by-wire which requires low-speed sensorless estimation. In [8], it was found that the handwheel of a commercial vehicle operates at mean zero speed with fast position changes at a maximum rate of 286 degrees/s. Such conditions have been generally found to be challenging for high-speed observers as the back-emf produced by the machine is low and of the same order of magnitude as sensor offsets and non-linearities. Hence, alternative techniques have to be used which rely on the injection of additional signals superimposed on the fundamental control ones [9].

The sensorless control of a salient PM machine using a rotating high-frequency vector was simulated in [1] and implemented experimentally on a 400 W 12 V surface-mounted PM synchronous machine (SMPMSM) in [10]. The simulation environment assumes an ideal salient machine with constant but different values of synchronous inductances $L_d$ and $L_q$. When converted to the alpha-beta or abc frames of reference, these inductances result in a rotor position-dependent tensor matrix due to saliency. The saliencies in simulation have a perfect sinusoidal variation; hence, the errors in the sensorless estimates are negligible. However, the saliencies observed on the experimental SMPMSM are not ideal; resulting in an error in the rotor mechanical position of 11.5° (error in the electrical domain 69°). This error is not suitable for vector-based current control of the machine, which aims to keep the stator and the rotor flux separate by 90° electrical. This paper models a sensorless observer in MATLAB which operates on the three-phase current data obtained from the experimental setup shown in [10]. The proposed observer uses selective real-time filtering in order to improve the quality of the saliencies measured in order to reduce the error in the position estimate.

## 2 Theory of saliency

### 2.1 Theory of saliency

The theory of saliency in a PMSM is derived from the flux equation assuming RFO given in (1). Transforming the inductance diagonal matrix from the synchronous frame to the $\alpha\beta$-frame the tensor given in (2) is obtained.

$$\begin{bmatrix}\Psi_{S_d}\\ \Psi_{S_q}\end{bmatrix} = \begin{bmatrix}L_d & 0\\ 0 & L_q\end{bmatrix}\begin{bmatrix}i_{S_d}\\ i_{S_q}\end{bmatrix} + \begin{bmatrix}\Psi_{R_d}\\ 0\end{bmatrix} \quad (1)$$

where, $\Psi_{S_d}/\Psi_{S_q}$ is the stator flux in the $d/q$-axis; $L_d/L_q$ is the stator inductance in the $d/q$-axis; $i_{S_d}/i_{S_q}$ is the stator inductance in the $d/q$-axis

$\Psi_{R_d}$ is the rotor flux in the $d/q$-axis



This is an open access article published by the IET under the Creative Commons Attribution-NonCommercial-NoDerivs License (http://creativecommons.org/licenses/by-nc-nd/3.0/)

20513305, 2019, 17, Downloaded from https://ietresearch.onlinelibrary.wiley.com/doi/10.1049/joe.2018.8248 by University Of Malta, Wiley Online Library on [13/03/2023]. See the Terms and Conditions (https://onlinelibrary.wiley.com/terms-and-conditions) on Wiley Online Library for rules of use; OA articles are governed by the applicable Creative Commons License

$$\begin{bmatrix} L_\alpha \\ L_\beta \end{bmatrix} = \begin{bmatrix} L - \Delta L\cos(2\theta_e) & -\Delta L\sin(2\theta_e) \\ -\Delta L\sin(2\theta_e) & L + \Delta L\cos(2\theta_e) \end{bmatrix} \quad (2)$$

where $L_\alpha/L_\beta$ is the stator flux in the $d/q$-axis

$$L = \frac{L_d + L_q}{2}$$

$$\Delta L = \frac{L_d - L_q}{2}$$

The tensor in (2) introduces a cross-coupling effect between α and $\beta$ axes.

### 2.2 Rotating voltage vector injection

The injection of a rotating voltage vector in the $\alpha\beta$ frame is performed by superimposing a high-frequency carrier in the form of (3) on the fundamental control voltage of the PMSM.

$$\begin{bmatrix} v_{i_\alpha} \\ v_{i_\beta} \end{bmatrix} = \begin{bmatrix} V_i\cos(\omega_i t) \\ V_i\sin(\omega_i t) \end{bmatrix} \quad (3)$$

where $V_{\rm i}$ is the amplitude of the injected HF component; $\omega_i$ is the frequency of the injected HF component.

The rotating voltage vector injection (3) results in a corresponding HF current in the PMSM with a saliency-dependent amplitude as shown in (4).

$$\begin{bmatrix} i_{i_\alpha} \\ i_{i_\beta} \end{bmatrix} = \begin{bmatrix} I_1\sin(\omega_i t) + I_2\sin(2\theta_e - \omega_i t) \\ -I_1\cos(\omega_i t) - I_2\sin(2\theta_e - \omega_i t) \end{bmatrix} \quad (4)$$

where

$$\mathrm{I}_1 = \frac{vi}{\omega_i}\frac{L}{L^2 - \Delta L^2}$$

$$\mathrm{I}_2 = \frac{vi}{\omega_i}\frac{\Delta L}{L^2 - \Delta L^2}$$

The sideband in the resulting $\alpha\beta$ HF currents due to saliency is on the negative side of the frequency spectrum around $-\omega_i$; hence, it can be easily demodulated. The performance of a PLL observer with a heterodyning demodulation input stage for a rotating voltage vector injection is discussed in [1, 10].

### 2.3 Physical contributors to saliency

The synchronous inductances $L_d$ and $L_q$ can be expressed in terms of the stator leakage inductances $L_{\rm ld}/L_{\rm lq}$ and the stator magnetising inductances $L_{\rm md}/L_{\rm mq}$ (5). The leakage inductance represents the slot, end-connection, and tooth-top leakage flux and the magnetising inductance represents the fundamental air-gap flux.

$$\begin{bmatrix} L_d \\ L_q \end{bmatrix} = \begin{bmatrix} L_{\rm ld} + L_{\rm md} \\ L_{\rm lq} + L_{\rm mq} \end{bmatrix} \quad (5)$$

The variation in the synchronous inductances in the $d$ and $q$ axes can be a result of variations in either one or both of the aforementioned inductances. The rotor geometry predominantly affects the magnetising inductance when the air gap is large compared to the stator slot opening. This effect is mostly observed in surface inset or partially insets magnets on the rotor core [11]. The magnetising inductances can be expressed in terms of form factors $k_{\rm fd}$ and $k_{\rm fq}$ as shown in (6) which are based on physical rotor constants [12].

$$\begin{bmatrix} L_{\rm md} \\ L_{\rm mq} \end{bmatrix} = \begin{bmatrix} k_{\rm fd}L_m \\ k_{\rm fq}L_m \end{bmatrix} \quad (6)$$

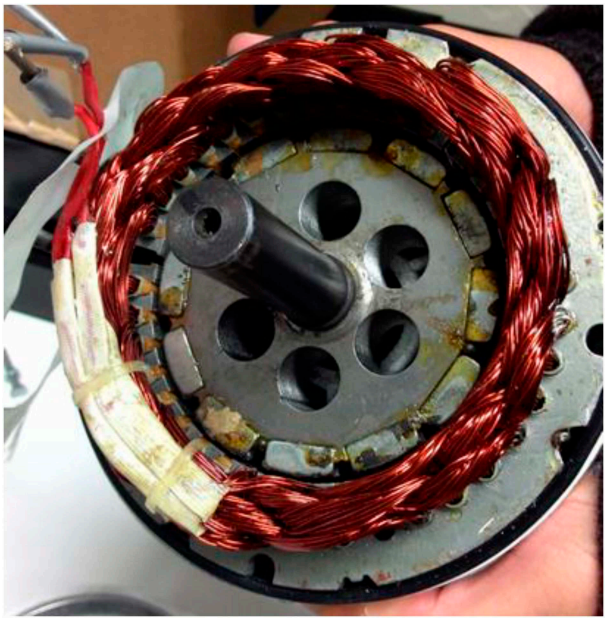

**Fig. 1** *12 V RMS 400 W 6-pole Surface Mounted Permanent Magnet Synchronous Machine*

Saturation is also another contributor to saliency and affects both the magnetising inductance and leakage inductance. Under no load conditions, the flux has a sinusoidal distribution along the air gap with a peak in the $d$-axis. This produces stator teeth saturation which increases the air gap in the $d$-axis resulting in a reduced $L_{\rm md}$, while $L_{\rm mq}$ remains unchanged. When the $q$-axis current is not zero, the term $L_m i_q$ shifts the distribution of the air gap in the $q$-axis direction. This shows that the saliency profile possibly changes under different load conditions [12]. The saturation in the machine's main flux also affects the stator leakage flux resulting in a spatial modulation of the leakage inductance. The main flux affects the stator teeth around the $q$-axis winding resulting in a reduction of $L_{\rm lq}$ while $L_{\rm ld}$ remains unchanged [12].

The identification of the exact physical contributors of saliency in the experimental SMPMSM requires detailed finite element analysis (FEA) which is beyond the scope of this paper. However, a visual inspection of the 12 V RMS 400 W 6 pole SMPMSM (Fig. 1) shows that the magnets on the rotor are of the partially inset type. Considering this and that, the size of the air gap is of considerable size when compared to the stator slot opening, could possibly result in a dominant rotor geometry-based saliency. Since the geometric saliency is dependent on the air gap, a low-cost machine such as the one used in this research with a high air-gap tolerance could contribute to the imperfect saliencies observed in [10]. The traditional inverse tangent or PLL-based observers cannot produce accurate estimates when operating directly on such non-sinusoidal inputs. Since saturation effects are also present to some extent, the sensorless observer used with this SMPMSM must also be designed for operation in dynamic load conditions.

## 3 Sensorless control theory

The high-frequency currents (4) resulting from the rotating voltage injection can theoretically be used directly with a PLL observer with a heterodyning section at its inputs shown in Fig. 2.

The error $\varepsilon$ resulting after heterodyning consists of a high- and a low-frequency component (7). The high-frequency component can be filtered out by a low-pass filter or by the closed-loop bandwidth of the PLL. The remaining low-frequency component is a function of the error between the actual and estimated rotor position.

$$\varepsilon = \mathrm{I}_1\sin(2(\omega_i t - \widehat{\theta}_e) + \mathrm{I}_2\sin(2(\theta_e - \widehat{\theta}_e) \quad (7)$$

The proportional integral (PI) controller within the PLL loop will reduce the error in the estimate to zero. By introducing an



This is an open access article published by the IET under the Creative Commons Attribution-NonCommercial-NoDerivs License (http://creativecommons.org/licenses/by-nc-nd/3.0/)

20513305, 2019, 17, Downloaded from https://ietresearch.onlinelibrary.wiley.com/doi/10.1049/joe.2018.8248 by University Of Malta, Wiley Online Library on [13/03/2023]. See the Terms and Conditions (https://onlinelibrary.wiley.com/terms-and-conditions) on Wiley Online Library for rules of use; OA articles are governed by the applicable Creative Commons License

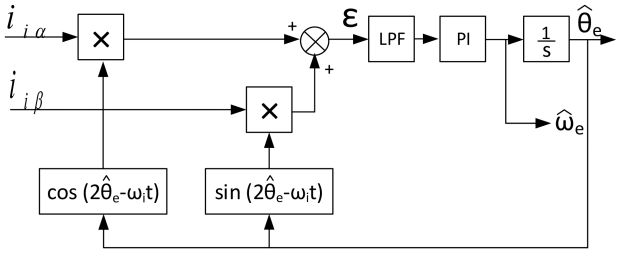


**Fig. 2** *PLL Observer with Heterodyning Input*

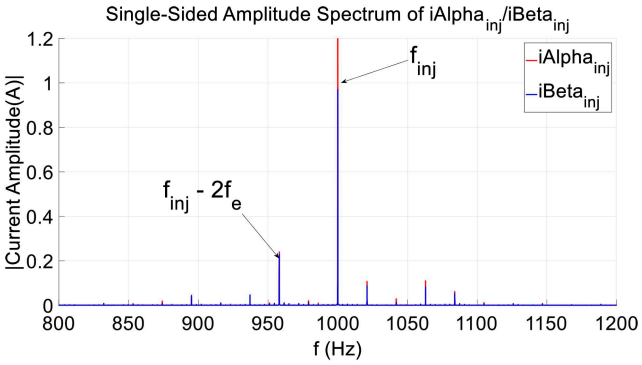


**Fig. 3** *Single-Sided Amplitude Spectrum of alpha-beta high frequency components*

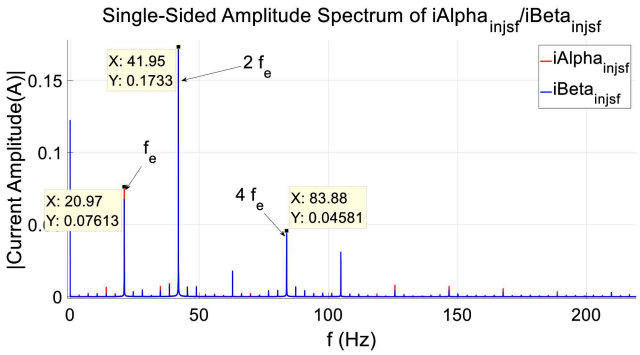


**Fig. 4** *Single-Sided Amplitude Spectrum of alpha-beta synchronous filtered components*

integrator block within the loop, the rotor rotational speed $\hat{\omega}_e$ is also obtained.

While in simulation [1], the observer shown in Fig. 2 has negligible estimation errors this in not the case in practice [10]. The error is a result of the saliencies in the $\alpha\beta$-frame not being perfectly sinusoidal. The frequency spectrum of the experimental high-frequency currents in the $\alpha\beta$ frame is shown in Fig. 3. From (4), only two components should exist at the injected frequency $f_{\text{inj}}$ and at the side-band depending on the rotor speed $f_{\text{inj}}$–$2f_e$. However, other frequency components can be observed in Fig. 3, which are the result of non-idealities such as air-gap variations in the electrical machine and switching losses in the inverter. The effects of these harmonics on sensorless position control have been researched for induction machines [13–15] and are still generally applicable to PMSMs [16–18]. The high-frequency currents are demodulated and filtered using a synchronous filter are shown in Fig. 4.

The demodulated ideal saliency component is at $2\,f_e$; however, other components are also present in Fig. 4. The most significant of these additional components are at $f_e$ and $4\,f_e$. If such saliency signals are used for estimation purposes directly, the rotor position estimate would be significantly deteriorated compared to the actual position. Hence, an enhanced sensorless estimation algorithm is required with adequate harmonic compensation such as space modulation profiling (SMP) [13]. In SMP, position-dependent look-up tables are generated to compensate for the non-linearities present causing distortion to the $2\,f_e$ component. The SMP

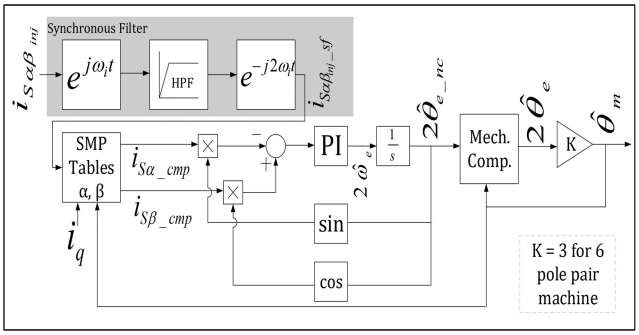


**Fig. 5** *Sensorless Estimator with SMP/Mechanical Compensation and PLL loop*

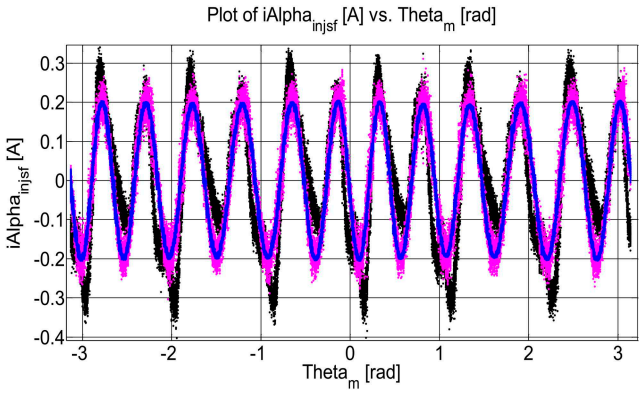


**Fig. 6** *Plot of Synchronous filtered alpha component [A] vs $\theta_m$ [rad] (Actual – black, Ideal – blue, Compensated – pink)*

approach has the drawback of requiring a zero-phase filter which cannot be computed in real time, thus requiring offline calibration.

The proposed observer with SMP table compensation is shown in Fig. 5. The high-frequency $\alpha\beta$ currents are demodulated and filtered using a synchronous filter. The outputs of the filter $i_{s\alpha\beta inj_{sf}}$ are compensated using SMP tables, which are applied as a function of both the mechanical rotor position $\theta_m$ and the $q$-axis current $i_{\text{q}}$. The compensated components $i_{s\alpha\beta_{comp}}$ are fed into the PLL observer without heterodyning (demodulation is carried out in the synchronous filter). The output of the PLL observer $2\widehat{\theta_{e_{nc}}}$ requires further mechanical compensation due to the pole-to-pole magnet and air-gap variations in the electrical machine. Both the electrical rotor position estimate $\widehat{\theta_e}$ and the relative mechanical rotor position estimate $\widehat{\theta_m}$ are available with the proposed observer.

## 4 Simulation results

The simulation results shown in this section are for the observer proposed in Section 3 modelled in MATLAB and operating on actual experimental measurements from the 400 W 12 V RMS SMPMSM. A rotating voltage vector with $V_i = 3.0$ V (25% of the DC-link voltage) and $f_{\text{inj}} = 1$ kHz was used on the experimental drive with a constant $i_q^* = 1$ A. The load machine (handwheel side) is driven at constant speed for test purposes.

The output of the synchronous-filtered $\alpha\beta$ components prior and post-SMP table compensation as a function of the mechanical rotor position $\theta_m$ are shown in Figs. 6 and 7. The compensated saliency components are visibly closer to the ideal single frequency sinusoidal component. This is a result of attenuation of the additional components shown in Fig. 4.

The actual and estimated rotor electrical position output from the observer 2 $\theta_e$ is shown in Fig. 8. The maximum error in the electrical rotor position is 2.8° (0.47° error in the rotor mechanical position). Such estimates are typically suitable for closed-loop sensorless control of the SMPMSM.


This is an open access article published by the IET under the Creative Commons Attribution-NonCommercial-NoDerivs License (http://creativecommons.org/licenses/by-nc-nd/3.0/)

20513305, 2019, 17, Downloaded from https://ietresearch.onlinelibrary.wiley.com/doi/10.1049/joe.2018.8248 by University Of Malta, Wiley Online Library on [13/03/2023]. See the Terms and Conditions (https://onlinelibrary.wiley.com/terms-and-conditions) on Wiley Online Library for rules of use; OA articles are governed by the applicable Creative Commons License

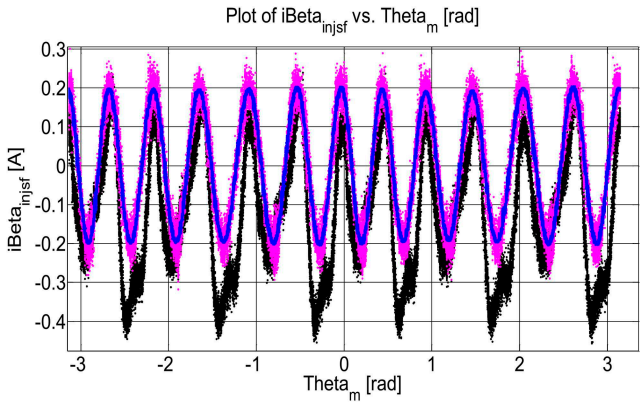


**Fig. 7** *Plot of Synchronous filtered beta component [A] vs $\theta_m$ [rad] (Actual – black, Ideal – blue, Compensated – pink)*

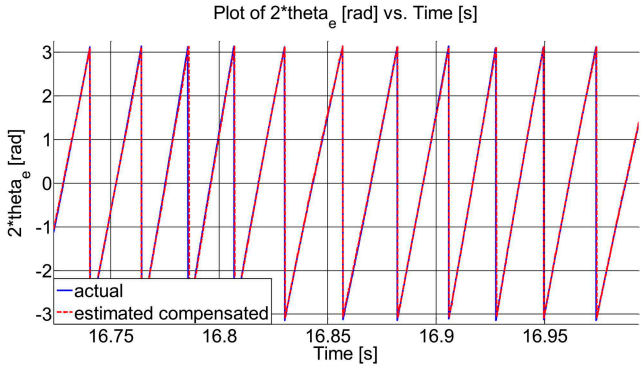


**Fig. 8** *Plot of 2 $\theta_e$ [rad] vs. Time [s]*

**Table 1** Error Comparison Table

| | error in $\theta_m$ est. [°] | error in $\theta_e$ est. [°] |
|---|---|---|
| PLL observer | 11.5 | 69 |
| SMP observer | 0.47 | 2.8 |

## 5 Conclusions

This paper has reviewed the application of sensorless control to the steer-by-wire application. In Section 1, the need for a backup rotor position measurement was identified for the required ASIL. The ideal theory of saliency of PMSMs was discussed in Section 2, and different possible contributors to physical machine saliency were identified. The low-cost machine used for this paper was found to have non-ideal sinusoidal saliency in previous research, which is possibly a result of high manufacturing tolerances in the air gap and physical PM dimensions. The imperfect saliencies were shown to produce a frequency spectrum with a number of unwanted harmonics, which significantly reduce the accuracy of traditional inverse tangent and PLL observers. Hence, a new sensorless observer using SMP table compensation and a simpler PLL configuration without heterodyning was proposed in Section 3. This observer also includes a mechanical compensation for pole-to-pole variations, which are not included in the SMP tables which compensate only for the electrical domain assuming that the physical poles repeat themselves exactly around the air gap of the machine.

The SMP table compensation was shown to significantly improve the $\alpha\beta$ saliency components being fed into the PLL observer in Section 4. The resulting errors in the rotor electrical/mechanical position for the SMP-based observer and for the traditional PLL observer in [10] are shown in Table 1. The performance of the proposed observer has significantly improved the estimates compared to the traditional PLL observer operating on non-compensated saliency signals as the error in the electrical rotor position was reduced by an order of magnitude from 69° to 2.8°.

While the performance of the proposed SMP-based observer is satisfactory for steer-by-wire applications, its practical implementation has a number of limitations. The SMP table approach only applies compensation in the electrical domain and further mechanical compensation is required for pole-to-pole variations. Both SMP and mechanical compensation are applied as a function of the previous known value of the rotor position; hence, an error due to noise in this parameter can lead the observer to become indefinitely unstable. The generation of SMP tables can only be carried out offline due to the zero-phase shift filter required. Furthermore, the estimate for the mechanical rotor position is relative and not absolute as required in the steer-by-wire application.

Presently, research is being carried out on the development of an innovative algorithm which produces sensorless estimates with the same level of accuracy as the SMP-based observer but with fewer practical limitations. The aim is to produce an algorithm which can be calibrated online without the use of a zero-phase shift filter in order to adapt to significant changes in machine parameters, while the drive is in operation. The algorithm is also intended to be optimised for different load conditions similarly to what was proposed in the SMP observer here.

## 6 References


[1] Scicluna, K., Staines, C.S., Raute, R.: 'Sensorless position control of a PMSM for steer-by-wire applications'. 2016 Int. Conf. on Control, Decision and Information Technologies (CoDIT), St. Julian's, Malta, 2016, pp. 046–051

[2] Bertoluzzo, M., Bolognesi, P., Bruno, O., *et al.*: 'Drive-by-wire systems for ground vehicles'. 2004 IEEE Int. Symp. on Industrial Electronics, Ajaccio, France, 2004, vol. 1, pp. 711–716

[3] Pimentel, J.R.: 'An architecture for a safety-critical steer-by-wire system'. SAE Technical Paper 0148-7191, 2004

[4] Bretz, E.A.: 'By-wire cars turn the corner', *IEEE Spectr.*, 2001, **38**, pp. 68–73

[5] Benedetti, A., Bianchi, N., Bolognani, S., *et al.*: 'PM motor drives for steer-by-wire applications'. Industry Applications Conf., 2005. Fourtieth IAS Annual Meeting. Conf. Record of the 2005, Kowloon, Hong Kong, 2005, vol. 4, pp. 2857–2864

[6] Bolognani, S., Tomasini, M., Zigliotto, M.: 'Control design of a steer-by-wire system with high performance PM motor drives'. IEEE 36th Power Electronics Specialists Conf., 2005 (PESC '05), Recife, Brazil, 2005, pp. 1839–1844

[7] Mariano, M., Scicluna, K., Scerri, J.: 'Modelling of a sensorless rotor flux oriented BLDC machine'. 19th Int. Conf. on Electrical Drives and Power Electronics (EDPE), Dubrovnik, Croatia, 2017

[8] Scicluna, K., Staines, C.S., Raute, R.: 'Torque feedback for steer-by-wire systems with rotor flux oriented PMSM'. 2017 19th Int. Conf. on Electrical Drives and Power Electronics (EDPE), 2017, pp. 188–193

[9] Staines, C.S., Caruana, C., Raute, R.: 'A review of saliency-based sensorless control methods for alternating current machines', *IEEJ J. Ind. Appl.*, 2014, **3**, pp. 86–96

[10] Scicluna, K., Staines, C.S., Raute, R.: 'Sensorless position tracking for steer-by-wire applications'. 2017 19th Int. Conf. on Electrical Drives and Power Electronics (EDPE), Dubrovnik, Croatia, 2017, pp. 341–346

[11] Gieras, J.F.: 'Permanent magnet materials and circuits', in Gieras, J.F. (Ed.): '*Permanent magnet motor technology: design and applications*' (CRC press, Boca Raton, FL, USA, 2002), pp. 45–88

[12] Silva, C.A.: 'Sensorless vector control of surface mounted permanent magnet machines without restriction of zero frequency', University of Nottingham, 2003

[13] Teske, N., Asher, G.M., Sumner, M., *et al.*: 'Analysis and suppression of high-frequency inverter modulation in sensorless position-controlled induction machine drives', *IEEE Trans. Ind. Appl.*, 2003, **39**, pp. 10–18

[14] Holtz, J., Hangwen, P.: 'Elimination of saturation effects in sensorless position-controlled induction motors', *IEEE Trans. Ind. Appl.*, 2004, **40**, pp. 623–631

[15] Teske, N., Asher, G.M., Sumner, M., *et al.*: 'Suppression of saturation saliency effects for the sensorless position control of induction motor drives under loaded conditions', *IEEE Trans. Ind. Electron.*, 2000, **47**, pp. 1142–1150

[16] Silva, C., Asher, G., Sumner, M.: 'An hf signal-injection based observer for wide speed range sensorless PM motor drives including zero speed'. Proc. EPE'03, Toulouse, France, 2003, pp. 1–9

[17] Silva, C., Asher, G., Sumner, M., *et al.*: 'Sensorless rotor position control in a surface mounted PM machine using HF rotating injection', *EPE J.*, 2003, **13**, pp. 12–18

[18] Silva, C., Asher, G.M., Sumner, M.: 'Hybrid rotor position observer for wide speed-range sensorless PM motor drives including zero speed', *IEEE Trans. Ind. Electron.*, 2006, **53**, pp. 373–378




This is an open access article published by the IET under the Creative Commons Attribution-NonCommercial-NoDerivs License (http://creativecommons.org/licenses/by-nc-nd/3.0/)

20513305, 2019, 17, Downloaded from https://ietresearch.onlinelibrary.wiley.com/doi/10.1049/joe.2018.8248 by University Of Malta, Wiley Online Library on [13/03/2023]. See the Terms and Conditions (https://onlinelibrary.wiley.com/terms-and-conditions) on Wiley Online Library for rules of use; OA articles are governed by the applicable Creative Commons License